Articles

Complexes of $Ir_3(CO)_3(\eta^5\text{-}C_9H_7)_3$ with Metal Fragment Electrophiles

Matthew C. Comstock, Teresa Prussak-Wieckowska, Scott R. Wilson, and John R. Shapley*

School of Chemical Sciences, University of Illinois, Urbana, Illinois 61801

Received June 10, 1996[⊗]

The reactions of C_{3v} $Ir_3(\mu\text{-}CO)_3(\eta^5\text{-}C_9H_7)_3$ (**1**) with various metal electrophiles yield the cationic tetranuclear clusters $[Ir_3\{M(PPh_3)\}(CO)_3(\eta^5\text{-}C_9H_7)_3][PF_6]$ (**2**, M = Cu; **3**, M = Ag; **5**, M = Au), $[Ir_3Tl(\mu\text{-}CO)_3(\eta^5\text{-}C_9H_7)_3][PF_6]$ (**4**), and $[Ir_3(HgR)(CO)_3(\eta^5\text{-}C_9H_7)_3][PF_6]$ (**6**, R = Ph; **7**, R = $W(CO)_3(\eta^5\text{-}C_5H_5)$). Compounds **5**−**7** are best prepared via compound **4**. The structures of compounds **4** and **5** have been determined by X-ray diffraction. The C_{3v} symmetry of the parent cluster **1** is maintained in the structure of **4**. The molecule consists of a triangle of iridium atoms, each edge of which has a bridging carbonyl oriented out of the plane in the same direction and each vertex of which has an η^5-indenyl ligand oriented toward the opposite side of the plane. The thallium atom adopts a face-capping mode of coordination on the same side of the triiridium plane as the three indenyl ligands and is encapsulated by the phenylene portions of the indenyl groups. The molecular structure of **5** consists of a $AuIr_3$ butterfly framework with a hinge angle of 153.63(3)° and the gold atom in a wingtip position. Each CO ligand is bonded in a terminal mode to one iridium center, with one CO ligand 'down' relative to the Ir_3 plane and two CO ligands 'up', flanking the Ir−Ir edge bridged by the $Au(PPh_3)^+$ fragment. The indenyl ligands take up positions opposite those of the CO ligands at each iridium center. The infrared and ^1H NMR spectra of compounds **2**, **3**, **5**, **6**, and **7** are all very similar and are fully consistent with the solid-state structure of **5**.

We have previously described the synthesis and characterization of $Ir_3(\mu\text{-}CO)_3(\eta^5\text{-}C_9H_7)_3$ (**1**) as well as the related mixed-metal clusters $Ir_{3-x}Rh_x(\mu\text{-}CO)_3(\eta^5\text{-}C_9H_7)_3$ (x = 1, 2).[1] The solid-state structure of the triiridium cluster **1** exhibits nearly C_{3v} symmetry with three edge-bridging CO ligands oriented toward one face of the Ir_3 triangle and the three η^5-indenyl ligands oriented toward the opposite face. In this form there is a resemblance of **1** to the well-known triplatinum clusters $Pt_3(\mu\text{-}CO)_3(PR_3)_3$, which react readily with a variety of metal fragment electrophiles.[2] We now report that addition of metal electrophiles to **1** generates the cationic species $[Ir_3E(CO)_3(\eta^5\text{-}C_9H_7)_3][PF_6]$, (**2**, E = Cu(PPh$_3$); **3**, E = Ag(PPh$_3$); **4**, E = Tl; **5**, E = Au(PPh$_3$); **6**, E = Hg(Ph); **7**, E = Hg{W(CO)$_3$(η^5-C$_5$H$_5$)}) (see Scheme 1). Compounds **5**, **6**, and **7** are most easily prepared from the thallium compound, **4**.

Scheme 1

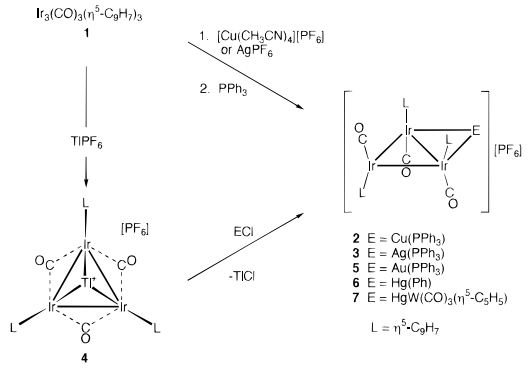

Experimental Section

General Procedures. All manipulations were conducted under an atmosphere of nitrogen by using standard Schlenk techniques. The triiridium cluster $Ir_3(CO)_3(\eta^5\text{-}C_9H_7)_3$ (**1**) was prepared from the reaction of $Ir(C_2H_4)_2(\eta^5\text{-}C_9H_7)$ with $Ir(CO)_2(\eta^5\text{-}C_9H_7)$ as described previously.[1] $[Cu(NCCH_3)_4][PF_6]$[3] and $HgCl\{W(CO)_3(\eta^5\text{-}C_5H_5)\}$[4] were prepared by literature methods. Triphenylphosphine (Aldrich), $TlPF_6$ (Strem), $AgPF_6$ (Aldrich), HgCl(Ph) (Alfa), and $AuCl(PPh_3)$ (Aldrich) were used without further purification. Solvents for preparative use were dried with the use of standard methods and distilled. The deuterated solvent, $(CD_3)_2CO$ (Cambridge Isotope Laboratories), was used as received.

Proton NMR spectra were recorded on a General Electric QE-300 spectrometer and referenced to residual solvent resonance (δ 2.04 for acetone-d_5). Phosphorus-31 NMR spectra were recorded at 121.6 MHz on a General Electric GN-300NB spectrometer and referenced to external 85% H_3PO_4. Infrared spectra were recorded on a Perkin-Elmer 1750 FT-IR spectrometer. UV−vis spectra were recorded on a Hewlett-Packard HP8452A diode array spectrophotometer. Mass

[⊗] Abstract published in *Advance ACS Abstracts,* August 1, 1997.

(1) Comstock, M. C.; Wilson, S. R.; Shapley, J. R. *Organometallics* **1994**, *13*, 3805.
(2) Imhof, D.; Venanzi, L. M. *Chem. Soc. Rev.* **1994**, 185.
(3) Kubas, G. J. *Inorg. Synth.* **1990**, *28*, 68.
(4) Mays, M. J.; Robb, J. D. *J. Chem. Soc. A* **1968**, 329.

S0276-7333(96)00460-8 CCC: $14.00

spectra were recorded on either a VG Quattro spectrometer (electrospray ionization, ES) or a VG ZAB-SE spectrometer (fast atom bombardment, FAB) by the staff of the Mass Spectrometry Laboratory of the School of Chemical Sciences. Microanalyses were performed by the staff of the Microanalytical Laboratory of the School of Chemical Sciences.

$[Ir_3\{Cu(PPh_3)\}(CO)_3(\eta^5\text{-}C_9H_7)_3][PF_6]$ (2). To a red CH_2Cl_2 solution (20 mL) of **1** (30.0 mg, 0.030 mmol) was added solid $[Cu(NCCH_3)_4][PF_6]$ (11.7 mg, 0.031 mmol), which resulted in an olive green solution. Peaks in the infrared spectrum at 1980 and 1945 cm^{-1} were observed. Addition of PPh_3 (8.6 mg, 0.033 mmol) with stirring led to a red-brown solution after 15 min. The solvent was removed, and the residue was left under vacuum for 8 h to remove any excess CH_3CN. The residue was redissolved in CH_2Cl_2, giving a green solution after stirring for 20 min. The solvent was removed again, and the residue was extracted with acetone at 0 °C, filtered to remove any remaining **1**, and then dried under vacuum. Finally, the residue was triturated with diethyl ether and again dried under vacuum. Yield: 36 mg (0.024 mmol, 80%). IR (ν_{CO}, CH_2Cl_2): 1981, 1951 cm^{-1}. Anal. Calcd for $C_{48}H_{36}CuF_6Ir_3O_3P_2$: C, 39.04; H, 2.46 Found: C, 38.84; H, 2.55. UV−vis (CH_2Cl_2, λ_{max} (ϵ)): 416 (sh, 7980), 608 (4820), 764 (2570) nm. ES-MS (CH_2Cl_2): *m/z* (^{63}Cu, ^{193}Ir) 1333 ($Ir_3\{Cu(PPh_3)\}(CO)_3(C_9H_7)_3^+$).

$[Ir_3\{Ag(PPh_3)\}(CO)_3(\eta^5\text{-}C_9H_7)_3][PF_6]$ (3). A solution of $AgPF_6$ (7.5 mg, 0.030 mmol) in 2 mL of CH_3CN was added to a red CH_2Cl_2 solution (20 mL) of **1** (30 mg, 0.030 mmol), which resulted in an olive green solution. Solid PPh_3 (7.8 mg, 0.030 mmol) was added, and the solution was stirred for 5 min. The solvent was removed, and the residue was left under vacuum for 3 h to remove any excess CH_3CN. The residue was redissolved in CH_2Cl_2, giving a green solution after stirring for 20 min. The solvent was removed again, and the residue was dissolved in acetone, filtered to remove any remaining **1**, and then dried under vacuum. Finally, the residue was triturated with diethyl ether and again dried under vacuum. Yield: 31 mg (0.020 mmol, 66%). IR (ν_{CO}, CH_2Cl_2): 1980, 1952 cm^{-1}. Anal. Calcd for $C_{48}H_{36}AgF_6Ir_3O_3P_2$: C, 37.90; H, 2.39. Found: C, 37.33; H, 2.52. UV−vis (CH_2Cl_2, λ_{max} (ϵ)): 404sh (10 470), 608 (5860), 768 (3070) nm. ES-MS (CH_3CN): *m/z* (^{107}Ag, ^{193}Ir) 1377 ($Ir_3\{Ag(PPh_3)\}(CO)_3(C_9H_7)_3^+$); 1114 ($Ir_3Ag(CO)_3(C_9H_7)_3^+$).

$[Ir_3Tl(\mu\text{-}CO)_3(\eta^5\text{-}C_9H_7)_3][PF_6]$ (4). To a red CH_2Cl_2 solution (15 mL) of **1** (84 mg, 0.084 mmol) was added solid $TlPF_6$ (27 mg, 0.077 mmol), and the mixture was stirred for 24 h. The red suspension was dried under vacuum, and the residue was washed with CH_2Cl_2 (3 × 10 mL) to remove any excess **1** and THF (3 × 10 mL) to remove excess $TlPF_6$. The resulting red powder was dried under vacuum. Yield: 64 mg (0.047 mmol, 61%). IR (ν_{CO}, Nujol) 1820, 1788, 1775 cm^{-1}. Partial digestion of solid **4** in boiling acetone and cooling to room temperature provided crystals suitable for X-ray diffraction and elemental analyses. Anal. Calcd for $C_{30}H_{21}F_6Ir_3O_3PTl\cdot CH_3C(O)CH_3$: C, 28.04; H, 1.93. Found: C, 27.83; H, 2.01. FAB-MS (3-NBA): *m/z* (^{205}Tl, ^{193}Ir) 1213 ($Ir_3Tl(CO)_3(C_9H_7)_3^+$).

$[Ir_3\{Au(PPh_3)\}(CO)_3(\eta^5\text{-}C_9H_7)_3][PF_6]$ (5). To a red suspension of **4** (64 mg, 0.047 mmol) in acetone (50 mL) was added solid $AuCl(PPh_3)$ (24 mg, 0.049 mmol). The mixture was stirred at room temperature for 24 h, resulting in a green supernatant over a white solid. The solvent was removed under vacuum, and the residue was extracted with CH_2Cl_2 (5 × 10 mL) through a filter cannula. The solvent was removed under vacuum, and the solid was washed with benzene (5 × 10 mL) to remove excess $AuCl(PPh_3)$. The residue was triturated with diethyl ether and dried under vacuum. Yield: 39 mg (0.024 mmol, 52%). X-ray quality crystals were formed at room temperature by dissolving the green solid in 2-butanone (5 mL) and adding a layer of hexane (5 mL). IR (ν_{CO}, CH_2Cl_2): 1986, 1954 cm^{-1}. Anal. Calcd for $C_{48}H_{36}AuF_6Ir_3O_3P_2$: C, 35.80; H, 2.25. Found: C, 35.67; H, 2.29. UV−vis (CH_2Cl_2, λ_{max} (ϵ)): 410 (sh, 9510), 618 (4530), 770 (3180) nm. ES-MS (CH_3CN): *m/z* (^{197}Au, ^{193}Ir) 1467 ($Ir_3\{Au(PPh_3)\}(CO)_3(C_9H_7)_3^+$).

Table 1. NMR Data for Compounds 2, 3, 5, 6, and 7

	^1H[a]					
compound	L[b]	H_2	H_1,H_3	J_{12} (Hz)	H_4−H_7, Ph[c]	^{31}P
2	L_1	5.26 (t)	5.73[d]	2.7	7.66−6.82	*P*Ph_3, 14.97 (s)
	L_2	5.87 (m)	6.17 (m)[d]			
3	L_1	5.46 (t)	5.83 (d)	2.7	7.72−6.70	*P*Ph_3, 18.80 (dd)[e]
	L_2	5.89 (m)	6.29 (m)			
			6.15 (m)			
5	L_1	5.53 (t)	5.85 (d)	2.7	7.80−6.69	*P*Ph_3, 51.90 (s)
	L_2	5.81 (m)	6.34 (d)			
			6.18 (m)			
6	L_1	6.02 (t)	6.05 (d)	2.6	7.68−7.07	
	L_2	5.98 (m)	6.57 (m)			
			6.37 (m)			
7[f]	L_1	5.96 (t)	6.04 (d)	2.7	7.67−7.33	
	L_2	5.86 (m)	6.50 (m)			
			6.27 (m)			

[a] The labeling scheme shown below was used for the assignments of the indenyl proton resonances. [b] The label L_1 refers to indenyl ligands bisected by a plane of symmetry, and the label L_2 refers to indenyl ligands in an asymmetric environment. [c] The resonances for H_4−H_7 and for the phenyl ligands, in those compounds that contain them, appear as overlapping multiplets. [d] The resonances for H_1 and H_3 are overlapped. [e] The phosphorus resonance for **3** appeared as two overlapping doublets: $^1J(^{109}Ag-^{31}P)$ = 632 Hz, $^1J(^{107}Ag-^{31}P)$ = 549 Hz. [f] For C_5H_5, δ 5.62s.

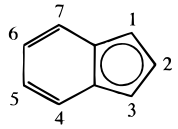

$[Ir_3\{HgPh\}(CO)_3(\eta^5\text{-}C_9H_7)_3][PF_6]$ (6). To a red suspension of **4** (31 mg, 0.023 mmol) in acetone (10 mL) was added solid Hg(Ph)Cl (7 mg, 0.023 mmol). The mixture was stirred at room temperature for 4 h, resulting in a blue-green supernatant over a white solid. The solvent was removed under vacuum, and the residue was extracted with CH_2Cl_2 (5 × 10 mL) through a filter cannula. The solvent was removed under vacuum. The residue was triturated with diethyl ether and dried under vacuum. Yield: 28 mg (0.020 mmol, 86%). IR (ν_{CO}, CH_2Cl_2): 2000, 1968 cm^{-1}. Anal. Calcd for $C_{36}H_{26}F_6HgIr_3O_3P$: C, 30.26; H, 1.83 . Found: C, 30.41; H, 2.28. UV−vis (CH_2Cl_2, λ_{max} (ϵ)): 404 (sh, 8260), 484 (sh, 3550), 590 (5660), 726 (2590) nm. ES-MS (CH_3CN): *m/z* (^{202}Hg, ^{193}Ir) 1287 ($Ir_3\{HgPh\}(CO)_3(C_9H_7)_3^+$).

$[Ir_3\{HgW(CO)_3(\eta^5\text{-}C_5H_5)\}(CO)_3(\eta^5\text{-}C_9H_7)_3][PF_6]$ (7). To a red suspension of **4** (30 mg, 0.022 mmol) in acetone (10 mL) was added an acetone solution of $HgCl\{W(CO)_3(\eta^5\text{-}C_5H_5)\}$ (10 mL, 0.0022 M, 0.022 mmol). The mixture was stirred at room temperature for 24 h, resulting in a green supernatant over a white solid. The solvent was removed under vacuum, and the residue was extracted with CH_2Cl_2 (5 × 10 mL) through a filter cannula. The solvent was removed under vacuum to give green microcrystals. Yield: 34 mg (0.020 mmol, 92%). IR (ν_{CO}, CH_2Cl_2): 1997, 1986, 1965, 1916, 1893 cm^{-1}. Anal. Calcd for $C_{38}H_{26}F_6HgIr_3O_6PW$: C, 27.09; H, 1.56 . Found: C, 26.77; H, 1.71 . UV−vis (CH_2Cl_2, λ_{max} (ϵ)): 424 (sh, 11 100), 490 (sh, 5370), 602 (6840), 740 (3310) nm. FAB-MS (3-NBA): *m/z* (^{202}Hg, ^{184}W, ^{193}Ir) 1543 ($Ir_3\{HgW(CO)_3(C_5H_5)\}(CO)_3(C_9H_7)_3^+$).

X-ray Structure Determination of 4. The red, transparent, prismatic crystal was mounted using oil (Paratone-N, Exxon) to a thin glass fiber. The 001 face of the crystal was damaged. Data were collected at 198 K on an Siemens Platform/CCD diffractometer. Crystal and refinement details are given in Table 2. Systematic conditions suggested the unambiguous space group $P6_3mc$. Scattering factors and

Table 2. Crystallographic Data for 4 and 5

	4	**5**
compound		
formula	$C_{30}H_{21}F_6Ir_3O_3PT_l$	$C_{48}H_{36}AuF_6Ir_3O_3P_2{\cdot}C_4H_8O$
fw	1355.41	1682.38
temperature	198(2) K	198(2) K
λ	0.710 73 Å (Mo Kα)	0.710 73 Å (Mo Kα)
space group, system	$P6_3mc$, hexagonal	$P2_1/a$, monoclinic
a	11.18680(10) Å	15.985(2) Å
b	11.18680(10) Å	13.438(3) Å
c	14.8013(2) Å	22.960(9) Å
α	90	90
β	90	99.86(2)
γ	120	90
V	1604.14(3) Å^3	4859(2) Å^3
Z	2	4
ρ_{calcd}	2.806 g cm^{-3}	2.30 g cm^{-3}
$F(000)$	1212	3128
cryst size	0.14 × 0.20 × 0.50 mm^3	0.24 × 0.18 × 0.12 mm^3
θ range	2.10−23.25°	1.76−23.47°
index ranges	$-9 \le h \le 12$, $-12 \le k \le 12$, $-16 \le l \le 13$	$-17 \le h \le 0$, $-15 \le k \le 0$, $-25 \le l \le 25$
I_{tot} (unique, R_i)	6076 (854, 0.1265)	7468 (7164, 0.0385)
abs corr, μ	integration, 17.526 mm^{-1}	integration, 11.334 mm^{-1}
max/min transmission	0.1426/0.0097	0.3360/0.1889
refinement method	full-matrix least-squares, F^2	full-matrix least-squares, F^2
data/restraints/parameters	854/7/81	7164/112/616
goodness of fit (F^2)[a]	1.006	1.238
R1[b], wR2 [$I > 2\sigma(I)$][c]	0.0349, 0.1100	0.0394, 0.0781
R1[b], wR2 (all data)[c]	0.0352, 0.1111	0.0944, 0.1141
ext coeff	0.0099(8)	0.00005(2)
largest diff peak and hole	+3.887 and −1.185 e Å^{-3}	+1.687 and −1.534 e Å^{-3}

[a] GOF = $[\sum[w(F_o^2 - F_c^2)^2]/(n-p)]^{1/2}$; n = number of reflections, p = total number of parameters refined. [b] R1 = $\sum||F_o| - |F_c||/\sum|F_o|$. [c] wR2 = $[\sum[w(F_o^2 - F_c^2)^2]/\sum[w(F_o^2)^2]]^{1/2}$.

anomalous dispersion terms were taken from standard tables.[5] The structure of **4** was solved by direct methods using the Siemens SHELXTL package of programs;[6−8] correct positions for the metal atoms were deduced from an *E*-map. One cycle of isotropic least-squares refinement followed by an unweighted difference Fourier synthesis revealed positions for the remaining non-H atoms. Hydrogen atoms were included as fixed idealized contributors. H atom *U*'s were assigned as $1.2U_{eq}$ of adjacent C atoms. Non-H atoms were refined with anisotropic thermal coefficients, except for the fluorine atoms of the PF_6 anion which were disordered between two sites. These were refined isotropically and the restrained to be octahedral with the P−F distances at 1.56 ± 0.02 Å. Successful convergence of the full-matrix least-squares refinement of F^2 was indicated by the maximum shift/error for the last cycle.[8] The highest peaks in the final difference Fourier map were in the vicinity of the metal atoms; the final map had no other significant features. The refined positional parameters are given in the Supporting Information.

X-ray Structure Determination of 5. The opaque, black, equidimensional crystal was mounted using oil (Paratone-N, Exxon) to a thin glass fiber. The faces and edges of the crystal were damaged. Data were measured at 198 K on an Enraf-Nonius diffractometer. Crystal and refinement details are given in Table 2. Systematic conditions suggested the unambiguous space group $P2_1/a$. Periodically monitored standard intensities showed 0.2% decay; no correction was applied. Step-scanned intensity data were reduced by profile analysis[9] and corrected for Lorentz−polarization effects and for absorption.[10] Scattering factors and anomalous dispersion terms were taken from standard tables.[5] The structure of **5** was solved by direct methods;[7] correct positions for the metal atoms were deduced from an *E*-map. One cycle of isotropic least-squares refinement followed by an unweighted difference Fourier synthesis revealed the positions for the remaining non-H atoms including one 2-butanone solvate molecule. Hydrogen atoms were included as fixed idealized contributors. H atom *U*'s were assigned as $1.2U_{eq}$ of adjacent C atoms. Non-H atoms were refined with anisotropic thermal coefficients. Carbon atoms coordinated to iridium atoms were restrained to be approximately isotropic (esd = 0.02). Owing to inaccuracy in the absorption correction, these C atom displacement parameters converged to chemically unrealistic values without restraints. Successful convergence of the full-matrix least-squares refinement of F^2 was indicated by the maximum shift/error for the last cycle.[8] The highest peaks in the final difference Fourier map were in the vicinity of the metal atoms; the final map had no other significant features. A final analysis of variance between observed and calculated structure factors showed dependence on amplitude. The refined positional parameters are given in the Supporting Information.

Results

Reactions of $Ir_3(\mu\text{-}CO)_3(\eta^5\text{-}C_9H_7)_3$ with Electrophiles. The addition of $[Cu(NCCH_3)_4][PF_6]$ to a red dichloromethane solution of **1** appeared to form an unstable green $[Cu(NCCH_3)]^+$ adduct. Prompt addition of triphenylphosphine generated $[Ir_3\{Cu(PPh_3)\}(CO)_3(\eta^5\text{-}C_9H_7)_3][PF_6]$ (**2**), which was isolated as a green solid in 80% yield. Similarly, the addition of triphenylphosphine to the reaction mixture of **1** and $AgPF_6$ in dichloromethane formed $[Ir_3\{Ag(PPh_3)\}(CO)_3(\eta^5\text{-}C_9H_7)_3][PF_6]$ (**3**), which was also isolated as a green solid. An attempt to prepare the analogous $[Au(PPh_3)]^+$ adduct showed that **1** does not react directly with $AuCl(PPh_3)$ in dichloromethane, but in the presence of $TlPF_6$, the desired compound $[Ir_3\{Au(PPh_3)\}(CO)_3(\eta^5\text{-}C_9H_7)_3][PF_6]$ (**5**) does form together with a highly insoluble red precipitate that has been characterized as $[Ir_3Tl(\mu\text{-}CO)_3$-

(5) *International Tables for X-ray Crystallography*; Wilson, A. J. C., Ed.; Kluwer Academic Publishers: Dordrecht, The Netherlands, 1992; Vol. C, (a) scattering factors, pp 500−502; (b) anomalous dispersion corrections, pp 219−222.
(6) *SHELXTL*, Version 5; Siemens Analytical X-Ray Instruments, Inc.: Madison, WI, 1994.
(7) Sheldrick, G. M. SHELXS-86. *Acta Crystallogr.* **1990**, *A46*, 467.
(8) Sheldrick, G. M. *SHELXL-93*; University of Göttingen: Göttingen, Germany, 1993.
(9) Coppins, P.; Blessing, R. H.; Becker, P. *J. Appl. Crystallogr.* **1972**, *7*, 488.
(10) Sheldrick, G. M. *SHELX-76. Program for crystal structure determination*; University of Cambridge: Cambridge, England, 1976.

(η^5-$C_9H_7)_3$][PF_6] (**4**). Compound **4** was generated directly from the combination of **1** and $TlPF_6$ in dichloromethane, and it is a useful intermediate for subsequent reactions in acetone (in which **4** is very slightly soluble) with AuCl(PPh_3), HgCl(Ph), and HgCl{$W(CO)_3(\eta^5$-$C_5H_5)$} to provide [Ir_3{$Au(PPh_3)$}$(CO)_3(\eta^5$-$C_9H_7)_3$][PF_6] (**5**), [Ir_3{HgPh}$(CO)_3(\eta^5$-$C_9H_7)_3$][PF_6] (**6**), and [Ir_3{HgW-$(CO)_3(\eta^5$-C_5H_5}$(CO)_3(\eta^5$-$C_9H_7)_3$][PF_6] (**7**), respectively, in good yields. These transformations are summarized in the Scheme 1.

The nature of **4** was especially intriguing, since it alone among the adducts formed retains the red color of precursor **1**. The FAB mass spectrum of **4** shows the molecular ion for [$Ir_3Tl(CO)_3(\eta^5$-$C_9H_7)_3^+$]. The infrared spectrum of **4** in Nujol exhibits peaks in the bridging carbonyl stretching region at 1820 (s, br), 1788 (m), and 1775 (m) cm^{-1}. In comparison, the analogous IR spectrum of **1** displays the same overall peak shapes, but shifted to lower energy at 1786, 1751, and 1731 cm^{-1} (see Figure S-1 in the Supporting Information).[1] These data imply the formation of a one-to-one adduct that maintains the C_{3v} geometry present in the trinuclear precursor, a fact confirmed by X-ray diffraction (see below).

The infrared spectra of the cationic clusters **2**, **3**, and **5** in dichloromethane solution show only terminal carbonyls present with absorption peaks near 1980 and 1950 cm^{-1}. All three clusters exhibit virtually identical spectra with little deviation in the frequencies of absorption (see Figure S-2, Supporting Information). These spectra suggest that **2**, **3**, and **5** adopt analogous structures in solution and that the identity of the coinage metal does not particularly affect the energy of the CO stretching frequencies. Similarly, the infrared spectrum for **6** has peaks at 2000 and 1968 cm^{-1}. Although the peaks are shifted to higher energy from those of the coinage metal adducts, the similar peak shapes suggest an analogous environment for the CO ligands. The infrared spectrum for **7** also has peaks in the same region as **6**; however, there is overlap of the Ir−CO bands with W−CO bands from the $W(CO)_3(\eta^5$-$C_5H_5)$ moiety.

The visible spectra of **2**, **3**, and **5** in dichloromethane are all closely comparable with shoulders at 410 ±6 nm and two broad features at 610 ±8 and 767 ±3 nm (see Figure S-3, Supporting Information). The visible spectrum of **6** has shoulders at 404 and 484 nm and two broad features at 590 and 726 nm. The visible spectrum of **7** is closely similar to that of **6**, with shoulders at 424 and 490 nm as well as two broad features at 602 and 740 nm.

The ^{1}H NMR spectra of **2**, **3**, **5**, **6**, and **7** in acetone are all very similar (see Table 1). The ^{1}H NMR spectrum of compound **5** and the effects of homonuclear decoupling are shown as representative examples in Figure 1. For each compound the spectrum exhibits two sets of indenyl resonances in a 2:1 ratio. The smaller set in each case indicates that the indenyl ligand resides in a symmetric environment. These spectra indicate a C_s geometry with a mirror plane that is perpendicular to the Ir_3 plane and passes through one iridium atom (and its indenyl ligand), the midpoint between the two remaining iridium atoms, and the heterometal. However, we cannot unambiguously deduce the specific solution structure of the compounds, since the butterfly

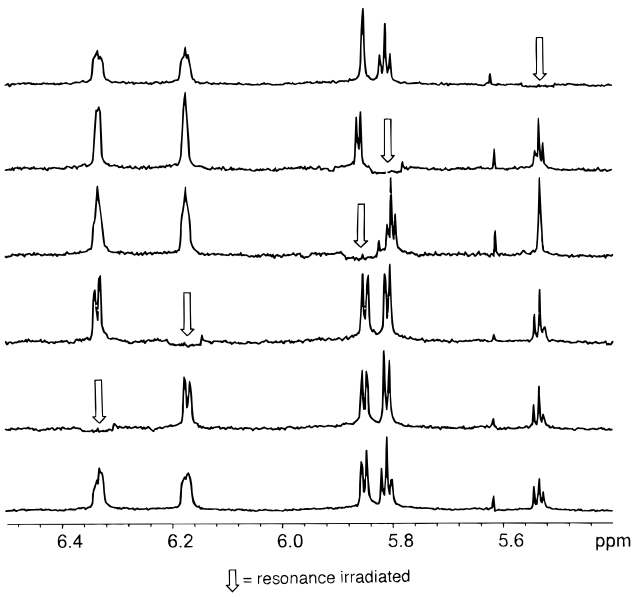

Figure 1. Proton NMR spectrum in acetone-d_6 of **5** (bottom), and proton NMR spectra of **5** including homonuclear decoupling (top 5 spectra).

geometries of both model I and II, which differ by a 180° rotation of the wingtip Ir(CO)(η^5-C_9H_7) vertex, are consistent with the NMR spectroscopy. This ambiguity

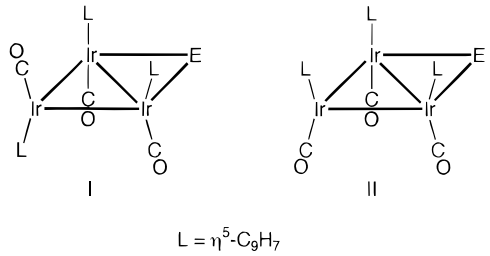

was resolved in favor of I by an X-ray crystallographic study of **5** (see below).

The phosphorus NMR spectra of **2**, **3**, and **5** are clearly dependent on the identity of the coinage metal. The chemical shifts of the phosphorus atoms attached to the coinage metals increase in the order Cu < Ag < Au. The phosphorus resonance in **3** is split into two doublets of approximately equal intensity due to spin−spin coupling with ^{109}Ag and ^{107}Ag (natural abundances of 48.65% and 51.35%, respectively), which confirms coordination of the phosphine ligand to the coinage metal. The ratio of the coupling constants $^1J(^{109}AgP)/^1J(^{107}AgP) = 632/549 = 1.15$, which is approximately the same as the ratio of the gyromagnetic ratios, $\gamma^{109}Ag/\gamma^{107}Ag$. The chemical shifts of the phosphorus nuclei in [Rh_3{μ_3-$M(PPh_3)$}(μ-$CO)_3(\eta^5$-$C_5H_5)_3^+$][11] and for other clusters containing μ-$M(PPh_3)$ units (M = Cu, Ag, Au)[12,13] also increase in the order Cu < Ag < Au; an appropriate splitting due to coupling with silver nuclei has been reported as well.

(11) Rybinskaya, M. I.; Kudinov, A. R.; Muratov, D. V.; Gambaryan, N. P.; Stankevich, I. V.; Chistyakov, A. L. *J. Organomet. Chem.* **1991**, *413*, 419.

(12) For examples, see: (a) Evans, J.; Stroud, P. M.; Webster, M. *Organometallics* **1989**, *8*, 1270. (b) Brice, R. A.; Pearse, S. C.; Salter, I. D.; Henrick, K. *J. Chem. Soc., Dalton Trans.* **1986**, 2181.

(13) (a) Salter, I. D. In *Comprehensive Organometallic Chemistry II*; Abel, E. W., Stone, F. G. A.; Wilkinson, G.; Adams, R. D., Eds.; Pergamon: New York, 1995; Vol. 10, Chapter 5. (b) Salter, I. D. *Adv. Organomet. Chem.* **1989**, *29*, 249.

Table 3. Selected Structural Data for the Cation 4

Internuclear Distances			
Ir1−Ir1′	2.7118(9)	Ir1−C1	2.00(2)
Ir1−Tl1	3.224(2)	C1−O1	1.17 (3)
Ir1−C11	2.15(2)	Tl1−C13	3.427(13)
Ir1−C12	2.232(14)	Tl1−C14	3.278(13)
Ir1−C13	2.478(14)	Tl1−C15	3.131(16)
Bond Angles			
Ir1−Tl1−Ir1′	49.74(3)	Ir1′−Ir1−Tl1	65.128(14)
C1−Ir1−Ir1″	47.4(5)	Ir1−C1−Ir1″	85.3(9)
Angles between Vectors and Planes			
C1,O1 vs Ir1,Ir1′,Ir1″			53.4

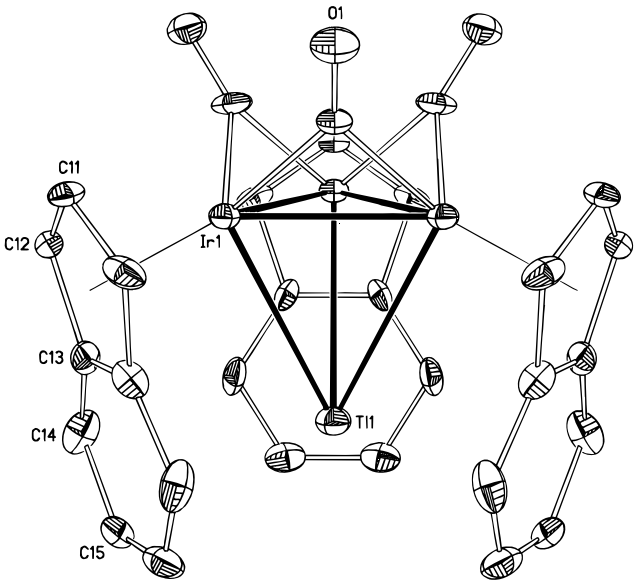

Figure 2. ORTEP diagram of the molecular structure of the cation **4**.

While compounds **5**, **6**, and **7** are stable in solution, compounds **2** and **3** are unstable toward loss of the $[M(PPh_3)]^+$ fragment, especially in polar solvents, and decompose within hours to give back **1**. Thus, the stability of the coinage metal adducts, $[Ir_3\{M(PPh_3)\}(CO)_3(\eta^5\text{-}C_9H_7)_3]$, increase in the order M = Cu < Ag < Au.

X-ray Crystal Structures of 4 and 5. The solid-state structure of **4** was determined by X-ray crystallography, and selcted results are given in Table 3. The cation consists of a triangle of iridium atoms, each edge of which has a bridging carbonyl ligand oriented out of the plane in the same direction and each vertex of which has an indenyl ligand oriented toward the opposite side of the plane (see Figure 2). The thallium atom adopts a face-capping mode of coordination on the same side of the Ir_3 plane as the indenyl ligands and is surrounded by the phenylene portions of the indenyl ligands. The molecule crystallizes in the hexagonal space group $P6_3mc$, and the structure was solved for the unique atoms Tl1, Ir1, C1, O1, and C11−C15 with the remaining atoms generated by symmetry. The Ir−Ir distance is 2.7118(9) Å, and the Ir−Tl distance is 3.224(2) Å. The individual Tl−C distances between the thallium atom and the carbon atoms of the six-membered ring of the indenyl ligand range are Tl−C13 = 3.427(13) Å, Tl−C14 = 3.278(13) Å, and Tl−C15 = 3.131(16) Å. The structural details of indenyl ligand bonding in $(\eta^5\text{-}C_9H_7)$M compounds can be described by the slip distortion parameter (Δ), the fold angle, and the hinge angle.[14] The values of these parameters for **4** are summarized in Table 5.

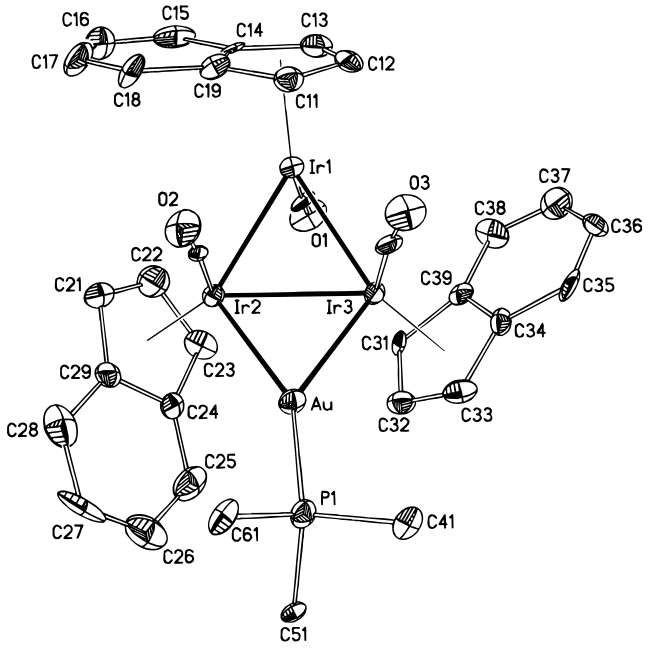

Figure 3. ORTEP diagram of the molecular structure of the cation **5**. Only the *ipso*-carbon atoms of the triphenylphosphine ligand are shown.

The solid state structure of **5** was determined by X-ray crystallography, and selected results are listed in Table 4. The cation consists of a $AuIr_3$ butterfly with the gold atom in a wingtip position and a hinge angle of 153.63(3)° (see Figure 3). Two of the Ir−Ir distances are similar, Ir1−Ir2 = 2.6534(12) and Ir1−Ir3 = 2.6788(10) Å, while the Ir−Ir bond bridged by the gold atom is longer, Ir2−Ir3 = 2.7630(9) Å. The bonding Au−Ir distances are 2.7103(11) and 2.7374(13) Å for Ir2 and Ir3, respectively (the nonbonding Au−Ir1 distance is 4.506(2) Å). The carbonyl ligands adopt a terminal mode of coordination, two on one side of the Ir_3 plane and one on the other. The indenyl ligand of the wingtip Ir atom lies over the same side of the Ir_3 plane as the gold atom, whereas the indenyl ligands on the two hinge Ir atoms lie over the other side of the Ir_3 plane. The slip distortion parameters, the fold angles, and the hinge angles for the indenyl ligands attached to Ir1, Ir2, and Ir3 are given in Table 5.

Discussion

The reactions of transition metal clusters with coinage metal fragments is a well-established method of increasing cluster nuclearity.[13] The use of Hg^{2+} reagents in the synthesis of higher nuclearity clusters has also been very successful.[15] Furthermore, bimetallic reagents, such as $HgCl\{M(CO)_3(\eta^5\text{-}C_5H_5)\}$, lead to clusters

(14) (a) Faller, J. W.; Crabtree, R. H.; Habib, A. *Organometallics* **1985**, *4*, 929. (b) Baker, R. T.; Tulip, T. H. *Organometallics* **1986**, *5*, 839. (c) Donovan, B. T.; Hughes, R. P.; Trujillo, H. A.; Rheingold, A. L. *Organometallics* **1992**, *11*, 64. (d) Kakkar, A. K.; Taylor, N. J.; Calabrese, J. C.; Nugent, W. A.; Roe, D. C.; Connaway, E. A.; Marder, T. B. *J. Chem. Soc., Chem. Commun.* **1989**, 990.

(15) (a) Rosenberg, E.; Hardcastle, K. I. In *Comprehensive Organometallic Chemistry II*; Abel, E. W., Stone, F. G. A., Wilkinson, G., Adams, R. D., Eds.; Pergamon: New York, 1995; Vol. 10, Chapter 6. (b) Gade, L. H. *Angew. Chem., Int. Ed. Engl.* **1993**, *32*, 24.

Table 4. Selected Structural Data for the Cation 5

		Internuclear Distances			
Ir1−Ir2	2.6534(12)	Au−Ir1	4.506(2)	Au−P1	2.234(4)
Ir1−Ir3	2.6788(10)	Au−Ir2	2.7103(11)		
Ir2−Ir3	2.7630(9)	Au−Ir3	2.7374(13)		
Ir1−C11	2.27(2)	Ir2−C21	2.19(2)	Ir3−C31	2.240(14)
Ir1−C12	2.21(2)	Ir2−C22	2.23(2)	Ir3−C32	2.25(2)
Ir1−C13	2.18(2)	Ir2−C23	2.25(2)	Ir3−C33	2.23(2)
Ir1−C14	2.303(14)	Ir2−C24	2.38(2)	Ir3−C34	2.31(2)
Ir1−C19	2.38(2)	Ir2−C29	2.33(2)	Ir3−C39	2.326(14)
Ir1−C1	1.83(2)	Ir2−C2	1.85(2)	Ir3−C3	1.83(2)
C1−O1	1.14(2)	C2−O2	1.15(2)	C3−O3	1.14(2)
P1−C41	1.80(2)	P1−C51	1.82(2)	P1−C61	1.81(2)
		Bond Angles			
Ir2−Au−Ir3	60.95(3)	Au−Ir3−Ir2	59.04(3)	Au−Ir2−Ir3	60.01(3)
Ir1−Ir3−Au	112.58(3)	Ir1−Ir2−Au	114.28(3)	Ir1−Ir2−Ir3	59.24(3)
Ir1−Ir3−Ir2	58.34(3)	Ir2−Ir1−Ir3	62.42(3)		
		Angles between Vectors and Planes			
	C1,O1 vs Ir1,Ir2,Ir3		83.4		
	C2,O2 vs Ir1,Ir2,Ir3		81.1		
	C3,O3 vs Ir1,Ir2,Ir3		74.8		
	Au,P1 vs Ir1,Ir2,Ir3		25.7		

Table 5. Crystallographic Characterization of Indenyl Ligand Distortion

compound	M[a]	Δ(slip), Å	fold, deg	hinge, deg	ref
1	Ir1	0.28	10.6	10.1	1
	Ir2	0.25	7.4	8.0	
	Ir3	0.27	12.3	10.5	
4	Ir1	0.25	6.3	5.5	this work
5	Ir1	0.12	5.1	5.3	this work
	Ir2	0.14	11.6	7.3	
	Ir3	0.08	10.7	5.9	
Ir(CO)(η^2-dmf)(η^5-C_9H_7)[b]	Ir	0.17	6.0	7.4	21

[a] Values in this column denote the indenyl ligand bonded to M. [b] η^2-dmf = dimethyl fumarate, *trans*-MeOC(O)CH=CHC(O)OMe.

containing pendant M(CO)$_3$(η^5-C_5H_5) units (M = Mo, W)[15,16] and enhance the range of metals combined.

Synthesis of Electrophile Adducts. The reactions of **1** with coinage metal or Hg^{2+} fragment electrophiles lead to cationic butterfly clusters **2**, **3**, **5**, **6**, and **7**, incorporating the electrophilic metal atoms in wingtip positions. The solid-state structure of **5** as determined by X-ray crystallography indicates the Ir_3 substructure has undergone a significant reorganization compared to the starting material **1**.[1] Aside from the three carbonyl ligands now adopting a terminal instead of bridging mode of coordination, the wingtip Ir(CO)(η^5-C_9H_7) vertex has been rotated by 180°. Close similarities among the spectroscopic data for these compoundssuggest that they all adopt analogous C_s structures in solution.

In other work,[17] we have observed that the reaction of **1** with HBF_4 also leads to a cation with C_s symmetry and that subsequent deprotonation forms a different isomer of **1** with C_s symmetry. The geometry of the latter is presumably similar to the structurally characterized compound $Ir_3(CO)_3(\eta^5\text{-}C_5H_5)_3$,[18] which has terminal carbonyl ligands and two η^5 ligands on one side of the Ir_3 plane and one on the other side. The C_{3v} and C_s isomers of **1** are in equilibrium in dichloromethane, with an equilibrium constant strongly favoring the C_{3v} form at 25 °C. Although the reaction pathway in the formation of the electrophile adducts **2**, **3**, **5**, **6**, and **7** is not clear, it is possible that the electrophilic reagents attack the C_s isomer preferentially, resulting in the observed geometries. However, attack upon the C_{3v} isomer and subsequent isomerization of the Ir_3 unit cannot be ruled out.

The results reported here stand in contrast to those reported for addition of electrophiles to C_{3v} $Rh_3(\mu\text{-}CO)_3(\eta^5\text{-}C_5H_5)_3$.[11,19] On the basis of ambient infrared and NMR spectroscopic data, both $[Rh_3(\mu_3\text{-}MPPh_3)(\mu\text{-}CO)_3(\eta^5\text{-}C_5H_5)_3^+]$ (M = Cu, Ag, Au)[11] and $[Rh_3(\mu_3\text{-}H)(\mu\text{-}CO)_3(\eta^5\text{-}C_5H_5)_3^+]$[19] were proposed to be C_{3v}-symmetric complexes of the electrophile.

It has been suggested[20] that the reason **1** adopts a structure containing three bridging carbonyl ligands rather than a structure with all terminal carbonyl ligands, as observed in $Ir_3(CO)_3(\eta^5\text{-}C_5H_5)_3$,[18] is due to a relatively large distortion of each indenyl ligand toward a trihapto (allylic) bonding mode. The distortion of indenyl ligands from an ideal η^5 mode of coordination in (η^5-C_9H_7)M compounds can be described by the slip distortion parameter (Δ), the fold angle, and the hinge angle, and compilations of these parameters for a variety of (η^5-C_9H_7)M and (η^3-C_9H_7)M systems have been made.[14] All of the entries in Table 5 show some degree of distortion. The degree of distortion in **1** is only marginally larger than that observed for the cationic compound **4**, although **5** and the mononuclear compound Ir(CO)(η^2-dmf)(η^5-C_9H_7) (dmf = dimethyl fumarate, *trans*-MeOC(O)CH=CHC(O)OMe)[21] do show smaller degrees of distortion. It is thus not truly clear how the indenyl ligand distortions may affect bridge vs terminal CO bonding.

The Ir−Tl distance of 3.224(2) Å in **4** is significantly longer than Pt−Tl distances observed in Pt_3 clusters

(16) For example, see: Reina, R.; Rossell, O.; Seco, M.; de Montauzon, D.; Zquiak, R. *Organometallics* **1994**, *13*, 4300.
(17) Comstock, M. C. Ph.D. Thesis. University of Illinois, Urbana, IL, 1996.
(18) Shapley, J. R.; Adair, P. C.; Lawson, R. J.; Pierpont, C. G. *Inorg. Chem.* **1982**, *21*, 1701.
(19) Herrmann, W. A.; Plank, J.; Riedel, D.; Ziegler, M. L.; Weidenhammer, K.; Guggolz, E.; Balbach, B. *J. Am. Chem. Soc.* **1981**, *103*, 63.
(20) Braga, D.; Grepioni, F.; Wadepohl, H.; Gebert, S.; Calhorda, M. J.; Veiros, L. F. *Organometallics* **1995**, *14*, 5350.
(21) Du, Y.; Shapley, J. R. Unpublished results.

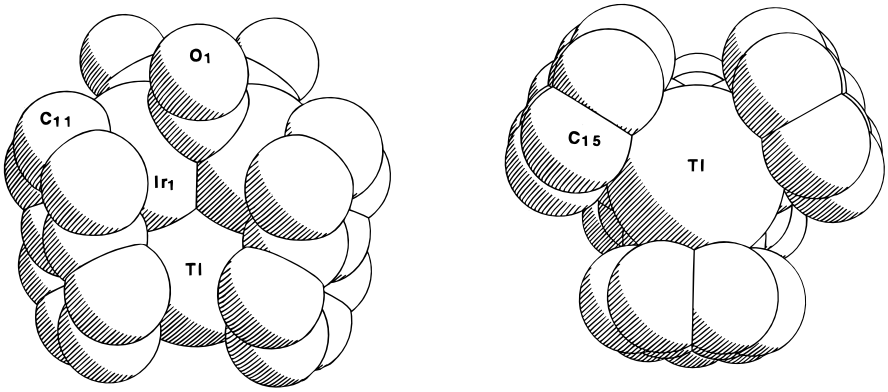

A B

Figure 4. Space-filling diagrams of the structure of **4**: (A) from the same perspective as that in Figure 2; (B) along the 3-fold axis.

containing face-bridging thallium atoms.[22] For example, in $[TlPt_3(CO)_3(PCy_3)_3][Rh(\eta\text{-}C_8H_{12})Cl_2]$ the thallium atom caps the Pt_3 face with an average Pt−Tl distance of 3.038(1) Å.[22a] More recently, the reaction of $TlPF_6$ with a compound containing two tethered Pt_3 triangles resulted in a cluster containing Tl bonded in a sandwich fashion to all six platinum atoms. The Pt−Tl distances ranged from 2.860(3)−2.992(3) Å.[22c] Using the shortest distance in the metal to approximate the covalent radius of Pt as 1.373 Å,[23] the effective covalent radius of Tl in the TlM_3 cluster $[TlPt_3(CO)_3(PCy_3)_3][Rh(\eta\text{-}C_8H_{12})Cl_2]$[22a] is 1.665 Å. With the covalent radius of Ir of 1.357 Å,[23] this leads to an expected Tl−Ir bond distance of 3.022 Å in an analogous $TlIr_3$ cluster. Compounds with Tl−Ir bonds are rare,[24] but comparison of the Ir−Tl distances of 2.958(1) and 2.979(1) Å in the A-frame compound $[Ir_2Tl(CO)_2Cl_2(\mu\text{-dpma})_2][NO_3]$[24a] offer further evidence for significantly long Tl−Ir interactions in **4**.

For compound **4**, the average distance between the thallium atom and the carbon atoms of the six-membered ring is 3.279 Å, and individual Tl−C distances range from 3.427(13) Å for Tl−C13 to 3.131(16) Å for Tl−C15. The interaction of the thallium ion with the six-carbon rings of the indenyl ligands resembles crystallographically characterized arene complexes of thallium.[25] For example, the structure of $[Tl(1,2,4\text{-}Me_3C_6H_3)_2][AlCl_4]$ has average Tl−C distances of 3.265 and 3.351 Å for the two different arene rings.[25e] Therefore, the interaction of the thallium with the Ir_3 face is accompanied by close Tl−C distances with the six-membered rings of the indenyl ligands. The encapsulation of the thallium ion is easily apparent in the space-filling views of **4** shown in Figure 4. However, despite this snug fit in the solid-state structure, the thallium ion is readily able to leave the pocket in acetone solution for the formation of compounds **5**−**7**.

It appears that the face-bridging configuration for **4** is favored by the significant interaction of the thallium ion with the π-electron 'pocket' created by the three indenyl ligands and that this interaction weakens the direct Tl−Ir bonds. It is unlikely, however, that such heterometallic bonding could be strong enough by itself to promote formation of the butterfly configuration favored by the other electrophile adducts, given the general reluctance of the $d^{10}s^2$ Tl(I) ion to form highly directional sigma bonds, i.e., the "inert pair effect".[26]

In the butterfly configuration adopted by **5**, two of the Ir−Ir distances are similar, Ir1−Ir2 = 2.6534(12) and Ir1−Ir3 = 2.6788(10) Å, while the Ir−Ir bond bridged by the gold atom is longer, Ir2−Ir3 = 2.7630(9) Å. The first two Ir−Ir distances are close to the average distance in **1** at 2.672 ± 0.006 Å[1] while the latter is significantly longer, consistent with the general observation for such coinage metal adducts that metal−metal bond distances increase upon interaction with a bridging fragment.[13] The bonding Au−Ir distances of 2.7103(11) and 2.7374(13) Å for Ir2 and Ir3, respectively, compare to the average Ir−Au distance of 2.837 Å in $[NMe_3(CH_2\text{-}Ph)][Ir_6(\mu\text{-}CO)_3(CO)_{12}\{\mu_3\text{-}Au(PPh_3)\}]$, which contains a face-capping $Au(PPh_3)$ unit,[27a] and the two Ir−Au distances of 2.788 and 2.731 Å in $Ir_4(CO)_{10}(\mu\text{-}PPh_2)(\mu\text{-}Au(PPh_3)$, which contains an edge-bridging $Au(PPh_3)$ unit.[27b] The $Ir_3(CO)_3(\eta^5\text{-}C_9H_7)_3$ substructure in **5** is analogous to the structure obtained for $Ir_3(CO)_3(\eta^5\text{-}C_5H_5)_3$.[18] This molecule exhibited two different Ir−Ir distances, two nearly identical at 2.6693(7) and 2.6697(6) Å, and one slightly longer at 2.6876(6) Å.

The transitions in the electronic spectra of green solutions of **2**, **3**, **5**, **6**, and **7** in dichloromethane all appear at similar energies with broad features near 600 and 750 nm. The visible spectrum of the green, C_s isomer of **1** also has peaks in the same region.[17] In contrast, the visible spectrum of red solutions of **1** in dichloromethane shows a strong, low-energy transition at 528 nm, which has been suggested as a metal−metal

(22) (a) Ezomo, O. J.; Mingos, M. P.; Williams, I. D. *J. Chem. Soc., Chem. Commun.* **1987**, 924. (b) Hao, L.; Xiao, J.; Vittal, J. J.; Puddephatt, R. J.; Manojlovic′−Muir, L.; Muir, K. W.; Torabi, A. A. *Inorg. Chem.* **1996**, *35*, 658. (c) Hao, L.; Vittal, J. J.; Puddephatt, R. J. *Inorg. Chem.* **1996**, *35*, 269.

(23) *CRC Handbook of Chemistry and Physics*, 71st ed.; Lide, D. R., Ed.; CRC: Boca Raton, FL, 1990−1991; Section 9, p 2.

(24) (a) Balch, A. L.; Nagle, J. K.; Olmstead, M. M.; Reedy, P. E., Jr. *J. Am. Chem. Soc.* **1987**, *109*, 4123. (b) Balch, A. L.; Neve, F.; Olmstead, M. M. *J. Am. Chem. Soc.* **1991**, *113*, 2995. (c) Van Vliet, P. I.; Vrieze, K. *J. Organomet. Chem.* **1977**, *139*, 337.

(25) (a) Schmidbaur, H. *Angew. Chem., Int. Ed. Engl.* **1985**, *24*, 893. (b) Schmidbaur, H.; Bublak, W.; Riede, J.; Müller, G. *Angew. Chem., Int. Ed. Engl.* **1985**, *24*, 414. (c) Noirot, M. D.; Anderson, O. P.; Strauss, S. H. *Inorg. Chem.* **1987**, *26*, 2216. (d) Frank, W.; Korrell, G.; Reiss, G. J. *Z. Anorg. Allg. Chem.* **1995,** *621*, 765. (e) Frank, W.; Korrell, G.; Reiss, G. J. *J. Organomet. Chem.* **1996**, *506*, 293.

(26) Greenwood, N. N.; Earnshaw, A. *Chemistry of the Elements*; Pergamon: Oxford, 1984; Chapter 7.

(27) (a) Pergola, R. D.; Demartin, F.; Garlaschelli, L.; Manassero, M.; Martinengo, S.; Masciocchi, N.; Sansoni, M. *Organometallics* **1991**, *10*, 2239. (b) Braga, D.; Grepioni, F.; Livotto, F. S.; Vargas, M. D. *J. Organomet. Chem.* **1990**, *391*, C28.

bonding to metal−metal antibonding transition.[1,20] It appears, therefore, that the gross features in the visible spectra of the electrophile adducts of **1** reflect the bonding in the triiridium subunit; discussion of further details, however, is deferred pending completion of our comparison of the two isomers of **1**.

Summary

The reactions of $Ir_3(\mu\text{-}CO)_3(\eta^5\text{-}C_9H_7)_3$ (**1**) with Cu^+ or Ag^+ sources followed by addition of PPh_3 provided $[Ir_3\{Cu(PPh_3)\}(CO)_3(\eta^5\text{-}C_9H_7)_3][PF_6]$ (**2**) and $[Ir_3\{Ag(PPh_3)\}(CO)_3(\eta^5\text{-}C_9H_7)_3][PF_6]$ (**3**), respectively, in high yields. The reaction of **1** with $TlPF_6$ provided the intriguing complex $[Ir_3Tl(CO)_3(\eta^5\text{-}C_9H_7)_3][PF_6]$ (**4**), which has been shown to have a thallium ion encapsulated by the six-membered rings of the indenyl ligands. Compound **4** was found to be a useful precursor in reactions with MCl reagents to provide the compounds $[Ir_3E(CO)_3(\eta^5\text{-}C_9H_7)_3][PF_6]$ (**5**, E = $Au(PPh_3)$; **6**, E = Hg(Ph); **7**, E = $Hg\{W(CO)_3(\eta^5\text{-}C_5H_5)\}$). Only adduct **4** maintains the C_{3v} geometry of precursor **1**, whereas the other adducts show rearrangement of the $Ir_3(\eta^5\text{-}C_9H_7)_3$ moiety to a C_s geometry.

Acknowledgment. This research was supported by the National Science Foundation (Grant No. CHE 94-14217). Purchase of the Siemens Platform/CCD diffractometer was supported by the National Science Foundation (Grant No. CHE 95-03145. M.C.C. thanks the Department of Chemistry for a fellowship funded by the Lubrizol Corporation. We thank Dr. Udo Brand and Kwangyeol Lee for help in solving the structure of compound **4**.

Supporting Information Available: Figures S-1, S-2, and S-3 comparing IR spectra of **1** and **4**, IR spectra of **2**, **3**, **5**, and **6**, and UV-visible spectra of **2**, **3**, **5**, and **6** and tables of atomic coordinates, bond distances and angles, and anisotropic displacement parameters from the crystallographic studies of **4** and **5** (14 pages). Ordering information is given on any current masthead page.

OM960460U